Structure and properties of polydisperse polyelectrolyte brushes studied by self-consistent field theory

Boris M. Okrugin[1,2], Ralf P. Richter[1,3],
Frans A.M.Leermakers[4], Igor M.Neelov[5,6],
Oleg V. Borisov[5,6,7], Ekaterina B. Zhulina[5,6]

[1]CIC biomaGUNE, Biosurface Lab, Paseo Miramon 182, 20014
San Sebastian, Spain
[2]St.Petersburg State University, Department of Physics,
198904 St.Petersburg, Russia
[3]University of Leeds, Faculty of Biological Sciences,
Faculty of Mathematics and Physical Sciences,
School of Physics and Astronomy and
Astbury Center for Structural Molecular Biology,
Leeds, LS2 9JT, United Kingdom
[4]Physical Chemistry and Soft Matter, Wageningen University,
6703 NB Wageningen, The Netherlands
[5]Institute of Macromolecular Compounds
of the Russian Academy of Sciences, 199004, St.Petersburg, Russia
[6]St.Petersburg National University of Informational Technologies,
Mechanics and Optics, 197101 St.Petersburg, Russia
[7]Institut des Sciences Analytiques et de Physico-Chimie pour
l'Environnement et les Matériaux, UMR 5254 CNRS UPPA,
Pau, France

June 3, 2018

Abstract

Two complementary self-consistent field theoretical approaches are

1

used to analyze equilibrium structure of binary and ternary brushes of polyions with different degrees of polymerization. Stratification in binary brushes is predicted: the shorter chains are entirely embedded in proximal sublayer depleted of end-points of longer chains while peripheral sublayer contains exclusively terminal segments of longer chains. The boundary between sublayers is enriched with counterions that neutralize residual charge of proximal sublayer. These analytical predictions for binary brushes are confirmed and extended to ternary brushes using numerical Scheutjens-Fleer approach.

1 Introduction

Polyelectrolyte (PE) brushes - layers of ionic macromolecules end-tethered at interfaces - are widely explored to control elastic, adhesive, and tribological properties of surfaces operating in contact with aqueous environment.[1–4] Because of the presence of charged monomer units, the brush-forming chains are capable of pronounced conformational response to variations in such environmental parameters as ionic strength and pH in the solution. Polydispersity of immobilized polyions could provide additional means to mediate the response of polymer monolayers.

Brushlike layers of ionized macromolecules are found as motives in natural objects.[5–9] For example, extracellular polymer coatings on microbial surfaces are composed primary of polysaccharides many of which are charged.[9] These layers are highly polydisperse and can have thickness up to few microns. Immobilized glycoproteins, such as mucins in periciliary layers in airways[6] and aggrecans in synovial joints[5] are composed of the core protein decorated by polysaccharide side chains. Polydispersity of mucins that are self-assembled from macromonomers, is evidently different from that in the bacterial extracellular layers. A distinct type of the brush polydispersity arises if the tethered macromolecules belong to protein family comprising of several isoforms, each with strictly monodisperse protein molecules. In this case polydispersity of the protein layer is dictated by stoichiometry of the participating isoforms. Typical examples are tau proteins that associate with and stabilize microtubules,[8] and neurofilament (NF) proteins that self-assemble in intermediate filaments in neuronal cells.[7]

The family of NF proteins comprises of three isoforms with different molecular weights, abbreviated as L (low), M (middle), and H (high). A typical self-assembled NF has a cylindrical core decorated by a brush of unstructured L, M, and H projection domains. *In vitro* experiments demonstrated that filament stoichiometry could be manipulated by varying concentrations of individual isoforms in solution.[10,11] Correspondingly, the brushes of projection domains in self-assembled L proteins or L co-assembled with M and H chains, would have quite different molecular weight distributions: strictly monodisperse in pure L filaments, bi-disperse in LM and LH filaments, and tri-disperse in LMH filaments incorporating all three components. Under "of cell" experimental conditions charge regulation in NF proteins could be performed by conventional means of physical chemistry,[12] i.e., by variations in pH and ionic strength in the solution. In this case, the equilibrium degree of protonation/deprotonation of amino acid residues is dictated by the local electrostatic potential, and the distribution of electric field becomes a major factor that determines the brush structure. The self-consistent field simula-

tions[13] has demonstrated that electrostatic potential in NF brushes exhibits distinct patterns associated with sublayers of short (L) and long (M, H) chains. That is, mono, bi- , and tri-dispersity of the molecular weight distribution directly translates in the NF brush structure and shape of the electrostatic potential profile. Therefore, understanding the relationship between polydispersity of macroions and structural organization of ionized polymer brushes is a fundamentally important problem for both artificial and natural PE brushes.

During the past two decades a robust "grafting from" approach has been established to create well-defined and sufficiently dense polyelectrolyte brushes.[14] The controlled radical polymerization techniques are usually employed for surface-initiated polymerization that gives rise to polymer and polyelectrolyte brushes with relatively narrow molecular weight distributions of brush-forming chains. Therefore, the results of experimental studies on structural and adhesive properties of PE brushes are usually rationalized on the basis of the existing theories for monodisperse polyions. The first scaling models[15–19] established the main regimes of PE brush behavior and specified power law dependences for brush characteristics under various solvent conditions, salt concentrations, and degrees of ionization. In addition, the theoretical studies based on the self-consistent field Poisson-Boltzmann approach[20–26] provided a more detailed description of the PE brush internal organization as well as distributions of mobile ions in salt-free and salt-added solutions.

The properties of non-ionic polydisperse and mixed polymer brushes have been thoroughly examined both theoretically and experimentally[27–37] (see also reviews[3,14]). However, the studies of polydisperse polyelectrolyte brushes are still rare. The aim of the present paper is to address the effect of polyion polydispersity by combining the analytical self-consistent field (SCF) approach with the numerical Scheutjens-Fleer (SF-SCF) modeling of binary and ternary PE brushes. The rest of the paper is organized as follows. We start with formulating an approximate analytical theory of binary PE brush developed in the strong-stretching (SS) approximation (Section 2). The predictions of the analytical theory are confronted to and supplemented by the results of the SF-SCF numerical modeling for binary and ternary PE brushes grafted to neutral surfaces (Section 3). Our conclusions are summarized in Section 4.

2 Analytical self-consistent field strong stretching approximation

2.1 Model

We consider binary brushes formed by strong polyelectrolytes with quenched (positive) fractional charge α per monomer unit and degrees of polymerization N_1 and N_2 ($N_2 > N_1$), respectively. The difference in molecular weights of shorter and longer chains in accounted for by mismatch parameter

$$\beta = \frac{N_2 - N_1}{N_1} \geq 0 \tag{1}$$

The fraction of longer chains (comprising of N_2 monomer units) in the brush is $q \leq 1$, and the fraction of shorter chains (comprising of N_1 monomer units) is $1 - q \leq 1$.
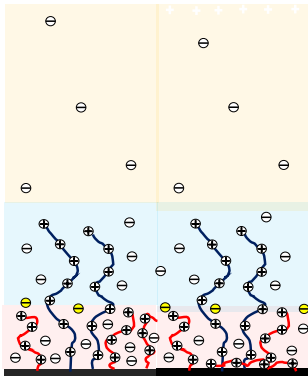

Figure 1: Schematics of binary polyelectrolyte brush.

The grafting density of polyions in the brush is $\sigma = 1/s$ (where s is the grafting surface area per chain). Hence partial grafting densities of long and short chains are $\sigma_2 = q\sigma$ and $\sigma_1 = (1-q)\sigma$, respectively, $\sigma = \sigma_1 + \sigma_2$. The chains are assumed to be intrinsically flexible, that is, the monomer unit size a coincides with the statistical segment length of the corresponding uncharged polymer. The latter is assumed to be on the order of the Bjerrum length $l_B = e^2/(\epsilon k_B T) \cong a$. The solution contains mobile monovalent counterions necessary to neutralize bare charge of the brush.

To investigate binary brushes of polyions we use the results of the analytical SS-SCF theory developed earlier for binary brushes of non-ionic macromolecules,[31] combined with the Poisson-Boltzmann framework to account for electrostatic interactions between charged species. This approach has been used previously to study one-component PE brushes.[20,24–26]

The analytical SS-SCF method incorporates the self-consistent molecular potential $U(x)$ acting at polymer chains in the brush.[38] The latter is governed by the presumed Gaussian elasticity of the tethered chains on all length scales. If intermolecular ionic interactions between charged monomer units and thermally equilibrated mobile ions dominate over other interactions in the system, the self-consistent electrostatic potential $\Psi(x)$ in a PE brush can be directly related to the molecular potential $U(x)$ as

$$\frac{U(x)}{k_B T} \approx \frac{\alpha e \Psi_{in}(x)}{k_B T} \equiv \alpha \psi_{in}(x) \qquad (2)$$

where $\psi_{in}(x) = e\Psi_{in}(x)/k_B T$ is the electrostatic energy of elementary charge e in the brush at distance x from the surface measured in $k_B T$ units and subscript "in" refers to the interior of the brush. It is termed below as dimensionless electrostatic potential.

Structural properties of a binary PE brush can be conveniently expressed using those of a reference one-component brush ($\beta = 0$) composed of polyions with length N_1 grafted with density $1/s$. This case has been treated in refs,[24,25] and we summarize below the relevant results.

2.2 One-component reference PE brush

We consider a monodisperse PE brush with thickness H_{ref} in contact with solution of 1:1 monovalent salt with concentration c_s. The latter specifies the Debye screening length in buffer solution as $\kappa^{-1} = (8\pi l_B c_s)^{-1/2}$. As long as polyelectrolyte chains exhibit the Gaussian elasticity, the self-consistent electrostatic potential inside the brush ($0 \leq x \leq H_{ref}$), can be presented as

$$\psi_{ref,in}(x) = \frac{H_{ref}^2 - x^2}{H_0^2} + C(\kappa) \tag{3}$$

where H_0 is the characteristic electrostatic length,[24]

$$H_0 = \sqrt{\frac{8}{3\pi^2}} N_1 \alpha^{1/2} a \tag{4}$$

and constant $C(\kappa)$ is introduced here to shift the reference state for electrostatic potential $\psi = 0$ from $x = H_{ref}$ to $x = \infty$. Its value is specified in eq 9 below. The reference state for the electrostatic potential with $\psi = 0$ at $x = \infty$ is conventional for salt-added solutions, and is also imposed in the numerical SF-SCF model which we use below to confront the analytical predictions.

Application of the Poisson equation,

$$\frac{d^2\psi_{ref,in}(x)}{dx^2} = -4\pi l_B \rho_{ref}(x) \tag{5}$$

allows for net charge density ρ_{ref} in the brush,

$$\rho_{ref}(x) = (2\pi l_B H_0^2)^{-1} \tag{6}$$

and residual (positive) charge per unit area

$$\tilde{Q}_{ref} = \int_0^{H_{ref}} \rho_{ref}(x)dx = \frac{H_{ref}}{2\pi l_B H_0^2} \tag{7}$$

The latter controls the Gouy-Chapman length

$$\tilde{\Lambda}_{ref} = \frac{1}{2\pi l_B \tilde{Q}_{ref}} = \frac{H_0^2}{H_{ref}}$$

of the counterion cloud outside the brush, i.e., at distances $x \geq H_{ref}$.

Outside of the brush, $x > H_{ref}$, the electrostatic potential $\psi_{ref,out}(x)$ coincides with that for a plane with surface (positive) charge number density $\tilde{Q}_{ref}$. It can be presented as[25]

$$\psi_{ref,out}(x) = 2\ln\left[\frac{(\kappa\tilde{\Lambda}_{ref} + \sqrt{(\kappa\tilde{\Lambda}_{ref})^2 + 1} - 1) + (\kappa\tilde{\Lambda}_{ref} - \sqrt{(\kappa\tilde{\Lambda}_{ref})^2 + 1} + 1)e^{-\kappa(x-H_{ref})}}{(\kappa\tilde{\Lambda}_{ref} + \sqrt{(\kappa\tilde{\Lambda}_{ref})^2 + 1} - 1) - (\kappa\tilde{\Lambda}_{ref} - \sqrt{(\kappa\tilde{\Lambda}_{ref})^2 + 1} + 1)e^{-\kappa(x-H_{ref})}}\right] \tag{8}$$

We remark that the potential defined by eq 8 vanishes at $x \to \infty$. The condition of continuity of the electrostatic potential at the brush edge, $\psi_{ref,out}(H_{ref}) = \psi_{ref,in}(H_{ref})$, provides the value of salt-dependent constant $C(\kappa)$ in eq 3,

$$C(\kappa) = -2 \ln \left[\frac{\sqrt{(\kappa \tilde{\Lambda}_{ref})^2 + 1} - 1}{\kappa \tilde{\Lambda}_{ref}} \right] \tag{9}$$

As it follows from eqs 3 and 9, the overall difference in the electrostatic potential between the grafting surface ($x = 0$) and $x = \infty$ arising because of the presence of the PE brush, $\Delta\psi = \psi(0) - \psi(\infty) = \psi(0)$, is given by

$$\psi(0) = \frac{H_{ref}^2}{H_0^2} + C(\kappa) = \frac{H_{ref}^2}{H_0^2} - 2 \ln \left[\frac{\sqrt{(\kappa \tilde{\Lambda}_{ref})^2 + 1} - 1}{\kappa \tilde{\Lambda}_{ref}} \right] \tag{10}$$

In low salt solution with $\kappa \tilde{\Lambda}_{ref} \ll 1$ constant $C(\kappa) \approx -2 \ln(\kappa \tilde{\Lambda}_{ref}/2)$, and $\psi(0)$ increases with the decrease in $\kappa \sim c_s^{1/2}$ as

$$\psi(0) \approx \frac{H_{ref}^2}{H_0^2} - 2 \ln(\frac{\kappa \tilde{\Lambda}_{ref}}{2}) = \frac{H_{ref}^2}{H_0^2} - 2 \ln \frac{\kappa}{2} - 2 \ln(\frac{H_0^2}{H_{ref}}) \tag{11}$$

As it follows from eqs 10 and 11, an increase in the degree of polymerization N of the tethered polyions weakly affects $\Delta\psi = \psi(0)$ at any fixed value of κ. As we demonstrate below, for system parameters typical for the osmotic brush regime, the increase in polyion length leads to a finite shift of $\psi(0)$ on the order of few percent. This quite weak increase in $\psi(0)$ is explained by accumulation of a larger amount of counterions in the brush with longer chains, and the corresponding reduction in the number of released counterions. Eq 10 can be used to determine the shift in $\psi(0)$ due to variations in molecular weight of the tethered polyions in both salt-added and salt-free solutions.

In the limit of salt-free solution $\kappa \sim c_s^{1/2} \to 0$ the polymer concentration profile, $c_{ref}(x)$, and the distribution of chain free ends, $g_{ref}(x)$, in one-component PE brush can be conveniently presented using reduced variables, $h_{ref} = H_{ref}/H_0$ and $t(x) = x/H_0$, as

$$c_{ref}(t) = (2\pi l_B \alpha H_0^2)^{-1}[1 + h_{ref}^2 \exp(h_{ref}^2 - t^2)] \tag{12}$$

$$g_{ref}(t) = \zeta_{ref}^{-1} \frac{t}{H_0} \left[\frac{1 + h_{ref}^2}{\sqrt{h_{ref}^2 - t^2}} + \sqrt{\pi} \exp(h_{ref}^2 - t^2) \mathrm{erf}(\sqrt{h_{ref}^2 - t^2}) \right] \tag{13}$$

Here,

$$\mathrm{erf}(y) = \frac{2}{\sqrt{\pi}} \int_0^y \exp(-z^2) dz$$

is the error function, and parameter ζ_{ref} is defined as

$$\zeta_{ref} = \sqrt{\frac{3}{2}} \alpha^{3/2} l_B N_1^2 \sigma a^2$$

The reduced thickness of the one-component reference brush, $h_{ref} = H_{ref}/H_0$, in salt-free solution is found from the normalization condition $\int_0^{H_{ref}} c_{ref}(x) dx = \sigma N_1$, and in the case of salt-free solution is specified by the equation

$$\zeta_{ref} = h_{ref} + h_{ref}^2 \frac{\sqrt{\pi}}{2} \exp(h_{ref}^2) \mathrm{erf}(h_{ref}) \tag{14}$$

2.3 Binary polyelectrolyte brush

Binary PE brush is obtained from the reference PE brush by extending fraction q of chains up to length $N_2 = N_1(1 + \beta)$. The analytical expression for the self-consistent molecular potential $U(x)$ in a binary non-ionic polymer brush was obtained in refs.,[27,31]

$$U(x) = \frac{3\pi^2}{8a^2 N_1^2} \begin{cases} u^2(H_{(n)}, H_{1(n)}) - x^2, & x \leq H_{1(n)} \\ u^2(H_{(n)}, H_{1(n)}) - u^2(x, H_{1(n)}), & H_{1(n)} \leq x \leq H_{(n)} \end{cases} \tag{15}$$

Here subscript (n) indicates neutral state of the brush, $H_{1(n)}$ is the thickness of sublayer of shorter N_1- chains, $H_{(n)}$ is the total brush thickness, while function $u(x, H_{1(n)})$ depends on mismatch $\beta = (N_2 - N_1)/N_1$ between molecular weights of short and long chains as

$$u(x, H_{1(n)}) = \frac{1}{(1 - \beta^2)} \left[x - \beta \sqrt{x^2 - (1 - \beta^2) H_{1(n)}^2} \right] \tag{16}$$

Molecular potential $U(x)$ in eq 15 ensures segregation of the end-points of non-ionic N_1- and N_2-chains: the former distribute their free ends in the proximal sublayer with thickness $H_{1(n)}$ while the latter delegate their free ends in the peripheral sublayer with thickness $H - H_{1(n)}$. The sizes of these two sublayers are governed by fraction q of longer chains. It was demonstrated[31] that in a non-ionic bidisperse brush the polymer density profile and distribution of the free ends in the proximal sublayer ($0 \leq x \leq H_{1(n)}$) coincide with those in a monodisperse brush of shorter N_1- chains. These analytical predictions were in good agreement with MC simulations.[33,40]

9

According to the analytical SS-SCF approach the molecular potential $U(x)$ in eq 15 is related to dimensionless electrostatic potential $\psi(x)$ in binary PE brush via eq 2. Making use of eqs 2, 4 we present the electrostatic potential ψ in a binary PE brush as

$$\psi_{1,2}(x) = \begin{cases} \psi_1(0) - \frac{x^2}{H_0^2}, & x \leq H_1 \\ \psi_1(0) - \frac{u^2(x,H_1)}{H_0^2}, & H_1 \leq x \leq H \end{cases} \tag{17}$$

Here, $\psi_1(0)$ is the value of electrostatic potential on the grafting surface, H_1 is the thickness of proximal to the grafting surface sublayer in which the shorter polyions are confined, H is the overall thickness of the brush, and β is the relative difference in molecular weights of long and short chains specified by eq 1. In a binary polyelectrolyte brush with $\beta \geq 0$ the thickness of proximal layer, $H_1 = H_1(q)$, and the overall thickness of the brush, $H = H(q)$, depend on the fraction of long and short chains in the brush. Here and below we use subscripts 1 and 2 to denote the brush properties in the proximal ($0 \leq x \leq H_1$) and the peripheral ($H_1 \leq x \leq H$) sublayers of binary PE brush, respectively. The proximal sublayer 1 contains all short chains and the stretched segments of long chains, and no free end-points of long polyions are found at $0 \leq x \leq H_1$.

At distances $x \geq H$ (i.e., outside the brush), the electrostatic potential is given by eq 8 in which $\tilde{\Lambda}_{ref}$ is substituted by the Gouy-Chapmann length $\tilde{\Lambda}$ governed by escaped from binary PE brush counterions. The condition of continuity of $\psi(x)$ at $x = H$ provides the ralationship between $\psi_1(0), u(H, H_1)$ and still unknown $\tilde{\Lambda}$ as

$$\psi_1(0) - \frac{u^2(H,H_1)}{H_0^2} + 2\ln\left(\frac{\sqrt{(\kappa\tilde{\Lambda})^2 + 1} - 1}{\kappa\tilde{\Lambda}}\right) = 0 \tag{18}$$

Electrostatic potential $\psi(x)$ in eq 17 exhibits two distinct features: (i) it is continuous at the boundary between sublayers, $x = H_1$; (ii) the first derivative $d\psi/dx$ which is proportional to the strength of electrostatic field, exhibits a jump at $x = H_1$ from a finite value at $x = H_1 - 0$ to zero at $x = H_1 + 0$. The latter condition indicates that in the framework of the analytical SS-SCF approach sublayer 1 is electroneutral.

By applying the Poisson equation, eq 5, and using eq 17 one finds net charge density in the brush as

$$\rho_{1,2}(x) = -\frac{1}{4\pi l_B}\frac{d^2\psi_{1,2}(x)}{dx^2} = (2\pi l_B H_0^2)^{-1} \begin{cases} 1, & 0 \le x < H_1 \\ \frac{d}{dx}\left(u(x,H_1)\frac{du(x,H_1)}{dx}\right), & H_1 < x \le H \end{cases}$$

(19)

As it follows from eq 19, net charge density $\rho^{(1)}(x) = \alpha c_1(H,x) - c_-^{(1)}(H,x)$ in the proximal sublayer 1 does not depend on distance x from the grafting surface and coincides with that in reference PE brush of N_1-chains (see eq 6), while net charge density $\rho_2(x)$ in the peripheral sublayer 2 is a decreasing function of x. Because net charge density is positive in sublayer 1 ($\rho^{(1)}(x) > 0$) while its net charge is zero, a finite number δQ_1 of mobile counterions per unit area become trapped between sublayers (at $x = H_1 - 0$) giving rise to an infinitely narrow double electric layer inside the brush. Evidently, this double layer disappears in monodisperse brushes of short ($q = 0$) and long ($q = 1$) chains. For values of $\beta \ne 1$ the net charge density $\rho(x)$ exhibits discontinuity at $x = H_1$.

The SS-SCF model therefore predicts that in addition to electric double layer at the brush edge ($x = H$) formed by escaped counterions, a second electric double layer comprising of a finite number δQ_1 of counterions per unit area forms inside the brush at the boundary between sublayers 1 and 2 ($x = H_1$). Although not fully accurate, eqs 2 and 15 offer a surprisingly good approximation for ψ in a binary PE brush, as demonstrated below by the numerical SF-SCF calculations.

According to eq 11 the shift δ in the electrostatic potential $\psi(0)$ in a monodisperse PE brush upon an increase in polyion length from N_1 to N_2 is given by

$$\delta = \psi_{N_2}(0) - \psi_{N_1}(0) = h_{ref}^2(N_2) - h_{ref}^2(N_1) + 2\ln\left(\frac{N_1}{N_2}\right) + 2\ln\left[\frac{h_{ref}(N_2)}{h_{ref}(N_1)}\right]$$

(20)

Here the reduced thicknesses $h_{ref}(N_2)$ and $h_{ref}(N_1)$ are obtained from eq 14 with the account of substitution $\zeta_{ref}(N_2) = (N_2/N_1)^2\zeta_{ref}(N_1) = (1+\beta)^2\zeta_{ref}(N_1)$.

In **Figure 2** the shift δ in $\psi(0)$ is plotted as a function of β for three values of $\zeta_{ref}(N_1) = 10$, 20, and 30, corresponding to the osmotic regime of salt-free reference brush composed of short polyions. As it is seen from fig. 2, in all cases δ initially rapidly increases with increasing β and then approaches the plateau with values of δ almost independent of β. The shift δ remains well below ten percent and decreases with increasing ζ_{ref}. Inset in fig. 2 demonstrates the shift δ as a function of reduced inverse Debye
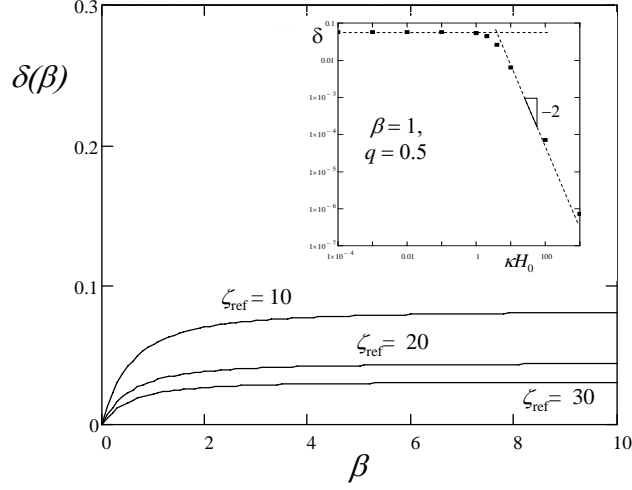
11

Figure 2: Shift δ in surface electrostatic potential, $\delta = \psi_{N2}(0) - \psi_{N1}(0)$ in a one-component brush with $N_2 = (1 + \beta)N_1$ as a function of β in salt-free solution. $\beta = 0$ corresponds to the reference brush of polyions with chain length N_1. Values of parameter $\zeta_{ref} = 10$ ($h_{ref} = 1.33$, $\zeta_{ref} = 20$ ($h_{ref} = 1.50$, $\zeta_{ref} = 30$ ($h_{ref} = 1.60$ indicated near the curves correspond to the reference brush formed by polyions of length N_1. Insert demonstrates dependence of δ on reduced Debye screening parameter κH_0 for $\beta = 1$ and $q = 0.5$.

length κH_0 for the values of $\zeta_{ref} = 10$ and $\beta = 1$ (i.e., $N_2 = 2N_1$). Two different regimes in δ-behavior are clearly seen. At low salt corresponding to $\kappa H_0 \ll 1$, δ does not depend on the salt concentration (which is indicative of the osmotic regime) and remains about 6%. At larger salt concentrations corresponding to $\kappa H_0 \gg 1$, δ rapidly decreases with apparent exponent -2. The absolute values of δ in both regimes decrease upon an increase in ζ_{ref}.

Clearly in a bidisperse brush containing fraction $q < 1$ of polyions with length $N_2 = N_1(1 + \beta)$, the shift $\delta(q)$ in the electrostatic potential $\psi(0)$ would be smaller compared to monodisperse brush formed by N_2-chains, $\delta(q) < \delta$. Therefore in the main, osmotic and salt-dominated regimes of binary PE brushes we could approximate (with accuracy of few percent) the electrostatic potential $\psi_1(0)$ in a binary PE brush as that in a reference brush of shorter N_1-chains,

$$\psi_1(0) = \psi(0) \approx \frac{H_{ref}^2}{H_0^2} - 2\ln\frac{\kappa}{2} - 2\ln(\frac{H_0^2}{H_{ref}}) \qquad (21)$$

The imposed in eq 21 independence of $\psi(0)$ of the brush composition q and mismatch β suggests a conjecture that similarly to non-ionic binary brushes,

12

the structure of proximal sublayer 1 coincides with that in a reference PE brush of N_1-chains. That is, the distribution function $g_1(x)$ of the free ends of shorter polyions,

$$g_1(x) \approx g_{ref}(x), \qquad 0 \leq x \leq H_1 \tag{22}$$

while polymer density profile in sublayer 1,

$$c_1(x) \approx c_{ref}(x), \qquad 0 \leq x \leq H_1$$

The normalization condition

$$\int_0^{H_1} g_1(x)dx = q \tag{23}$$

together with eqs 22 and 13 allow for thickness H_1 of sublayer 1 in binary PE brush. Introduction of the reduced thickness $h_1 = H_1/H_0$ of proximal sublayer 1 reduces eq 23 to

$$\sqrt{h_{ref}^2 - h_1^2} + \frac{\sqrt{\pi}}{2} h_{ref}^2 \exp(h_{ref}^2 - h_1^2)\mathrm{erf}(\sqrt{h_{ref}^2 - h_1^2}) = \zeta_{ref} q \tag{24}$$

As it follows from eq 24, the reduced thickness h_1 monotonously decreases as a function of q from $h_1 = h_{ref}$ at $q = 0$ to $h_1 = 0$ at $q = 1$. In the framework of the imposed approximation h_1 is independent of β, i.e., independent of length N_2 of the longer chains.

The Gouy-Chapmann length $\tilde{\Lambda}$ in eq 18 can be evaluated as follows. Because sublayer 1 does not contribute mobile counterions in the peripheral sublayer 2, electric double layer at the brush boundary $x = H$ is created only by counterions escaped from sublayer 2. Their number per unit area,

$$\widetilde{Q}_2 = \int_{H_1}^H \rho_2(x)dx = \frac{1}{2\pi l_B H_0} u(H, H_1)\left(\frac{du(x, H_1)}{dx}\right)_H$$

specifies the Gouy-Chapman length $\widetilde{\Lambda}$ for the tail of escaped counterions as

$$\widetilde{\Lambda} = \frac{1}{2\pi l_B \widetilde{Q}_2} = H_0 \frac{1}{u(h, h_1)\left(\frac{du(t, h_1)}{dt}\right)_h} \tag{25}$$

Therefore, eqs 17, 21 and 25 specify the total thickness H of binary PE brush.

The electrostatic potential ψ in a binary PE brush has therefore three distinct regimes than can be traced via the SF-SCF numerical calculations that incorporate the exact numerical solution for ψ on the Poisson-Boltzmann level. In the following section we address the assumptions adopted above by confronting the analytical predictions with the results of SF-SCF model. The details about SF-SCF approach can be found elsewhere (see, e.g., ref.[39]).

3 Numerical SF-SCF model of binary and ternary PE brushes

3.1 Binary PE brush

We now present the data of SF-SCF numerical calculations that provide a more detailed picture of binary PE brush structure.

3.1.1 Electrostatic potential.

In **Figure 3** we present the electrostatic potential ψ as a function of x^2 calculated for different fractions $q = 0$, 0.1, 0.3, and 0.5 of longer polyions with fixed length N_2 in a binary PE brush. For selected value of $q = 0.1$ the boundaries between different regimes of ψ are indicated by arrows. In sublayer 1 (i.e., at $x < H_1$), $\psi(x^2)$ demonstrates almost perfect straight line consistent with eq 17. In sublayer 2 ($H_1 < x < H$), the parabolic dependence of ψ with diminished numerical prefactor $(1 + \beta)^{-2}$ is recovered in the vicinity of the upper boundary of this regime, $x = H$. Here, the slopes of $\psi(x^2)$ (indicated by solid lines with the corresponding color) remain almost the same for different values of q, consistent with the analytical estimate in eq 17. The brush boundary $x = H$ is estimated from the deviation of the $\psi(x^2)$ dependence from the straight line due to the counterion tail extended to distances $x > H$.

In **Figures 4a and 4b** we present the electrostatic potential ψ calculated for fixed fraction $q = 0.5$ of longer polyions with varying molecular weights of longer chains N_2. In accordance with the expectations, position H_1 of the first sublayer (indicated in Figures 4a and 4b) does not change with an increase in N_2, and the electrostatic potential $\psi_1(x^2)$ in the proximal sublayer 1 is described by a straight line, common for all values of N_2. An increase in N_2 leads to the shift of the parabolic segment of ψ_2 (indicated by dashed lines in Figure 4a) to larger values of x accompanied by the decrease in slope of $\psi_2(x^2)$. Both observations are consistent with eq 17.

In Figure 4b the same data is plotted as a function of x^2 for $x \leq H_1$ and as a function of $u^2(x)$ for $x \geq H_1$ with value of H_1 adopted from fig. 4a. In accordance with eq 17 the SF-SCF data collapse on a common straight line confirming the predicted in eq 17 shape of ψ_2. Deviations of ψ from the straight line correspond to entering the region of the counterion tail ($x \geq H$), the position of the brush edge $x = H$ are indicated for different values of N_2 by the circles.

14

3.1.2 Structural properties.

We now focus on the equilibrium structural properties of binary PE brushes in more details. The effect of increasing length N_2 of longer chains on the structure of binary PE brush is illustrated in **Figures 5a-5b** in which we present partial (that is, for short and long chains separately) monomer density profiles and the chain ends distributions in binary brushes with a fixed fraction $q = 0.5$ of longer chains. Similar trends upon an increase in length N_2 of longer polyions are observed if the fraction q of longer chains in a binary PE brush is fixed at values 0.1 and 0.3 (not shown). As it is indicated by the density profiles and chain ends distributions in Figures 5, the two-layer structure of the brush is apparent at $N_2 \geq N_1$. Upon an increase in N_2 (at fixed $q = 0.5$) the peripheral sublayer 2 becomes more extended, whereas the density distributions for short and long chains (and, consequently their sum) in the proximal sublayer 1 remain unchanged. The position of the boundary between sublayers 1 and 2 remains independent of the length N_2 of longer chains as well. Remarkably the concentration of monomer units of shorter chains in sublayer 1 decreases as a function of distance from the grafting surface and vanishes at the boundary between the two sublayers, whereas the concentration of monomers of longer chains increases as a function of x within sublayer 1 and decreases within sublayer 2.

A divergence of the distribution function of the chain ends at the brush edge $x = H$ (as described by eq 13 for monodisperse PE brushes) is smeared out by the thermal fluctuations and is manifested as a characteristic shoulder in $g_2(x)$ close to the edge of the brush (see Figures 5b, 5d). The overall chain ends distribution in binary PE brush exhibits two distinct maxima corresponding to the end-points of shorter and longer chains, respectively. As it is seen in Figure 5b, there is almost no overlap between partial distributions of the chain ends: all the end-points of the shorter polyions are found in sublayer 1, with no ends of longer chains. All the end-points of longer chains are in the peripheral sublayer 2. This observation validates the two-layer model exploited above by the analytical SS-SCF theory. The distribution of free ends as well as partial density profiles for shorter chains in sublayer 1 are not affected by increasing length of the longer polyions.

The net charge densities inside and outside the brush are presented in **Figure 6**. The shapes of net charge density profiles $\rho(x)$ presented in Figure 6 demonstrate reasonable agreement with expectations of the analytical theory: The net charge density is low (positive) and virtually constant within each sublayer, and exhibits a sharp local minimum at the boundary between sublayers 1 and 2. The appearance of this minimum points to accumulation of counterions in a narrow cloud localized at the boundary between the layers.

These counterions neutralize the residual charge of the sublayer 1. Another cloud of counterions which neutralize the residual charge of sublayer 2 is located beyond the edge of brush.

In **Figure 7** we examine the effect of varying fraction of long chains q on the brush structure. In this case the lengths of both short and long chains are kept constant ($N_1 = 150$ and $N_2 = 500$), but fraction q of longer chains in the brush increases from $q = 0$ (reference one component brush) to $q = 0.5$. As one can see from Figure 7, the monomer density profile in the proximal sublayer 1 remains nearly identical to that in a reference brush, but an increase in q leads to the progressive decrease in width H_1 of sublayer 1, in accordance with eq 24. The partial distributions of the free ends of long and short chains do not overlap, and the distribution of the ends of short chains in the inner layer remains identical to that in a reference brush and only the width of the inner layer, which serves as the cut-off length for the distribution of the shorter chain ends, is displaced to smaller values of x upon an increase in q. The distribution of the free ends of longer chains is qualitatively similar to that in a one-component brush, i.e., exhibits a broad maximum and a characteristic shoulder close to the edge of the brush. The overall thickness of the brush is an increasing function of q which is a result of decreasing width of sublayer 1 accompanied by the increasing width of sublayer 2.

In **Figure 9** we compare the numerical SF-SCF results with predictions of eq 24 for thickness H_1 of the proximal sublayer as a function of fraction q of longer chains in binary PE brush. In the SF-SCF calculations H_1 was estimated from the position of maximum in net charge density distribution at the boudary between sublayers. As one can see from the figure, the approximate analytical theory reasonable well describes the q-dependence of the proximal layer thickness as log as the fraction of long chains remains below ≈ 0.5.

The response of the binary PE brush to variations in the ionic strength (controlled by added in the solution monovalent salt) is illustrated in **Figure 10**. As we can see from Figure 10, binary PE brush retains two-layer (stratified) structure upon an increase in the salt concentration. As expected, at low and moderate salt concentrations the proximal sublayer of the brush remains intact while the peripheral sublayer contracts, and the characteristic shoulder in the distribution of end-points of long chains disappears. Further increase in the salt concentration results in contraction of the proximal sublayer and progressive displacement of the boundary between sublayers towards the grafting surface.

3.2 Ternary PE brush

To explore further the effect of polydispersity on structural properties of PE brushes we have performed SF-SCF calculations for ternary brushes comprising of the chains with three different lengths, $N_1 \leq N_2 \leq N_3$, in equal proportion. We start with the reference brush with $N_1 = N_2 = N_3 = 300$ and then progressively diminish the value of N_1 from 300 to 250 and simultaneously increase the value of N_3 from 300 to 350 by keeping constant $N_2 = 300$ and $N_1 + N_2 + N_3 = 900$.

As one can see in **Figure 11a**, the increasing polydispersity has minor effect on the overall density profiles, which remain close to that in the reference monodisperse brush. Close inspection indicates, however, that the polymer concentration profile progressively changes the shape from convex to concave and the total thickness of the brush slightly increases.

The evolution of the cumulative distribution of the chain ends shown in **Figure 11b** is more pronounced, and at sufficiently large polydispersity one can distinguish three modes (three maxima) in the distribution that can be ascribed to three populations of the polyions. The analysis of partial density profiles and partial chain ends distributions presented in respective **Figures 11c** and **11d** unambiguously points to stratification of the brush into three sublayers: all the end segments of short, medium and long chains are found in the proximal, middle and peripheral sublayers, respectively. Remarkably, at small polydispersity, $\Delta N = N_3 - N_2 = N_2 - N_1 = 10$, the partial distributions of the chain ends are considerably overlapped. However, an increase in ΔN up to 50 results in substantial narrowing of the overlapping zones. The boundaries between sublayers become sharper indicating the appearance of three distinctive modes in the cumulative end segments distribution. Remarkably, partial end-point distributions for short and medium chains are nearly symmetric whereas the ends distribution for long chains keeps characteristic for a PE brush shape with a shoulder close to the brush edge.

The PE brush stratification is manifested also in partial density profiles presented in fig.11c. The density profile of the short chains retains the same shape as in a one-component brush or as in the proximal sublayer in the binary PE brush. Partial density profiles of the medium and long chains both have the shape similar to that of the density profile of long chains in a binary brush: they are non-monotonic and pass through maxima at the boundaries of the corresponding sublayers.

Finally, in **Figure 12** the net charge density profile in ternary brush is presented. Similarly to the case of binary PE brushes, the charge density exhibits sharp minima at the boundaries between sublayers, whereas it remains fairly constant within each sublayer. Remarkably, the minima become

deeper and sharper (narrower) upon an increase in ΔN, but for each value of ΔN minimum at the boundary between the peripheral and middle sublayers remains deeper than that at the boundary between the proximal and middle sublayers.

4 Discussion and Conclusions

In the present paper we have investigated the effect of bi- and tri-dispersity of long charged macromolecules on structural and responsive properties of planar polyelectrolyte brushes. We focused here on the analysis of PE brush structure in low salt solutions in which the long-range ionic interactions are manifested at most. An approximate two-layer analytical model correctly predicts the general trends in the binary PE brush behavior. That is, vertical stratification of the free ends of short and long polyions and formation of intermediate electric double layer at the boundary between the sublayers. The analytical theory provides a reasonable description of the electrostatic potential profile in PE brush, and of the sublayer comprised of shorter polyions. The predictions of approximate analytical theory are systematically compared to the results of numerical SF-SCF modelling. By using the SF-SCF approach we have also studied conformational response of binary PE brushes to variations in ionic strength in the solution.

The numerical SF-SCF calculations confirm that binary PE brushes exhibit stratification and segregation of the end-points of short and long chains into proximal and peripheral sublayers, respectively. The thickness of proximal sublayer of short chains is controlled by fraction q of long chains, but is independent of their length, N_2. The relative width of the boundary between sublayers, specified as an overlap zone between distributions of short and long chains, decreases upon an increase in the difference between N_1 and N_2.

The stratified organization of binary PE brush determines its specific response to external stimuli. We have demonstrated that moderate increase in the ionic strength in the solution affects primarily the conformations of long chains in peripheral layer, whereas short chains retain their extension up to high salt concentrations.

An interesting outcome of the theory is the prediction of electric double layer with accumulation of counterions at the boundary between sublayers of short and long polyions. The cumulative (negative) charge of these counterions matches residual (positive) charge of the proximal sublayer. These features, i.e., stratification (segregation) of the free ends of polyions with different lengths, and accumulation of counterions at the boundaries between

sublayers are observed also for ternary brushes that allowed us to anticipate that they are inherent for multicomponent polyelectrolyte brushes.

Similarly to the case of non-ionic brushes, the end-point distributions of polyions with close degrees of polymerization become strongly overlapped upon approaching the limit of continuous chain polydispersity, and the polymer density profile changes its shape from convex to concave.

We are currently unaware of the experimental realizations of synthetic bi- and tri- disperse PE brushes on which we could check our theoretical predictions. However, the theoretical results obtained in this study might provide insights in the results of *in vitro* experiments on NF proteins in solutions. Although the presented theory is formulated for planar PE brushes, the shape of electrostatic potential $\psi(z)$ remains the same in the cylindrical geometry of a binary PE brush provided that depletion of the free chain ends near cylindrical core (appearance of dead zone) is neglected. Moreover, while an absolute value of $\Delta\psi = \psi(0)$ decreases upon additions of salt in the solution, the shape of $\psi(z)$ would not change if the tethered polyions remain noticeably stretched. Therefore, predominant accumulation of counterions in sublayer of short chains as well as at the internal boundary in a binary PE brush is feasible in a wide range of conditions.

In case when in addition to monovalent counterions a small amount of divalent counterions is added into the solution, their accumulation inside PE brush is expected even at rather small concentrations $c_{2,bulk}$ in the solution. For example, the ratios of average concentrations c_2 of bivalent counterions in sublayer of shorter chains to the bulk value $c_{2,bulk} \ll c_s$ in a binary PE brush with values of the parameters: $N_1 = 150$, $N_2 = 500$, $\alpha = 0.2$, $q = 0.4$, $\sigma = 0.001$, were estimated by the SF-SCF calculations as $c_2/c_{2,bulk} \approx 25$ under low salt conditions ($c_s = 10^{-3}M$, $c_{2,bulk} = 10^{-5}M$), and $c_2/c_{2,bulk} \approx 2$ under high salt conditions ($c_s = 10^{-1}M$, $c_{2,bulk} = 10^{-3}M$). Note that latter conditions are close to physiological ones. As we discuss below, the accumulation of bivalent counterions in a PE brush might be responsible for the enhanced internal cross-bridging in NF filaments in solutions.

In vitro association of NF proteins in intermediate filaments and formation of hydrogel networks are thoroughly investigated experimentally (see, e.g.,[41] and references therein). It is established that short L chains are obligatory for self-assembly of NF isoforms in solutions.[10,11] Predominance of L chains in the mixed filaments suggests an estimate for the fraction of long chains as $q \simeq 0.4$.[43] Due to higher absolute values of the electrostatic potential in sublayer of short L chains, it accumulates counterions that could mediate local protonation/deprotonation of amino acid residues. The sublayer of L chains could also attract bivalent (e.g., Ca^{++}, Mg^{++}) counterions from the solution, that are believed to participate in cross-linking attributed

to M and H projection domains.[42]

The *in vitro* experiments performed on filaments composed of L and M proteins (no H chains in the solution) demonstrated that osmotic pressure - interfilament distance profiles in solutions of pure L and mixed LM filaments are practically identical.[11] In particular, $L-L$ and $LM-LM$ repulsions start at almost the same threshold interfilament distance, pointing at close values of the NF brush thickness in individual L and mixed LM filaments. In the first approximation the projection domains of L proteins can be envisioned as negatively charged polyelectrolytes with number of monomer units $N_1 = 142$ and the average degree of ionization $\alpha_L \simeq 0.25$. The projection domains of M proteins can be envisioned as negatively charged polyelectrolytes with number of monomer units $N_2 = 504$, and the average degree of ionization $\alpha_M \simeq 0.1 - 0.15$, depending on the level of their phosphorylation.[43] The latter values are less but close to the degree of ionization α_L of L projection domains. According to the theory presented in this paper, large mismatch $\beta = (N_2 - N_1)/N_1 \simeq 2.5$ in molecular weights of almost equally ionized L and M projections would lead to a larger thickness of individual LM filament compared to pure L filament unless the additional, not accounted in the theory interactions (e.g., cross-bridging) come into play.

The observed similarity of pressure-distance profiles for L and LM filaments[11] suggests that the extended conformations of M chains in LM filaments could change to resemble the typical conformations of L chains. In particular, in a dilute solution with non-interacting LM filaments, M chain could bend backwards with its terminal carboxyl segment penetrating sublayer of L chains, and making internal cross-links promoted by the accumulated bivalent ions in sublayer of L chains. Although such bending is unfavorable electrostatically and decreases also conformational entropy of M chains, overall increase in the free energy could be overruled by the free energy gain due to cross-links incorporating hydrophobic aminoacid residues, leading eventually to looped configurations of M chains in LM filament, stabilized by bivalent counterions. An increase in the solution osmotic pressure decreases the average distance between filaments and could trigger bridging attraction with (partial) substitution of internal cross-links by interfilament cross-bridges, and formation of hydrogel network of LM filaments.

The proposed (hypothetical) arguments to rationalize similarity of pressure-distance profiles in aqueous solutions of L and LM filaments are consistent with the established *in vivo* cross-bridging mechanism incorporating whole projection domains of M proteins.[44] A more quantitative comparison between the theory and experiments could be performed on mixed brushes of L and M projections, designed similar to already existing monodisperse brushes of H projections.[45]

Acknowledgements

References

[1] W.-L. Chen, R. Cordero, H. Tran and C. K. Ober, *Macromolecules*, 2017, **50**, 4089-4113.

[2] J. D. Willott, T.J. Murdoch, G.B. Webber and E.J.Wanless, *Progress in polymer science*, 2017, **64**, 52-75.

[3] R. Toomey and M.Tirrell, *Ann. Rev. Phys. Chem.,* 2008, **59**, 493-517.

[4] U. Raviv, S. Giasson, N. Kampf, J.-F. Gohy, R. Jerome and J. Klein, *Nature*, 2003, **425**, 163-165.

[5] C. Kiani, L. Cheng, Y.J. Wu, A.J. Yee and B.B. Yang, *Cell Research*, 2002, **12**, 19-32.

[6] B. Button, L.-H. Cai, C. Ehre, M. Kesimer, D.B. Hill, J.K. Sheehan, R.C. Boucher and M. Rubinstein, *Science*, 2012, **337**, 937-941.

[7] A. Laser-Azogui, M. Kornreich, E. Malka-Gibor and R. Beck, *Current Opinion in Cell Biology,* 2015, **32**, 92–101.

[8] J. Chen, J., Y. Kanai, N.Y. Cawan and N. Hirokawa, *Nature,* 1992, **360**, 674–677.

[9] B. Vu, M. Chen, R. J. Crawford and E.P. Ivanova, *Molecules* 2009, **14**, 2535-2554.

[10] J. B. Jones and C. R. Safinya, *Biophys. J*, 2008, **95**, 823–835.

[11] R. Beck, J. Deek and C. R. Safinya, *Biochem. Soc. Trans.,* 2012, **40**, 1027–1031.

[12] S. Kumar and J.H. Hoh, *Biochemical and Biophysical Research Communications,* 2004*,* **324**, 489–496.

[13] F.A.M. Leermakers and E.B. Zhulina, *Eur. Biophys. J.* 2010, **39**, 1323-1334.

[14] J. Ruhe, M. Ballauff, M. Biesalski, P. Dziezok, F. Gruhn, D. Johannsmann, N. Houbenov, N. Hugenberg, R. Konradi, S. Minko, M. Motornov, R.R. Netz, M. Schmidt, C. Seidel, M. Stamm, T. Stephan, D. Usov and H. Zhang, *Adv.Polym. Sci.,* 2004, **165**, 79-150.

[15] P.A. Pincus, *Macromolecules,* 1991, 24, 2912-2919.

[16] O.V. Borisov, T.M. Birshtein and E.B. Zhulina, *J.Phys. II* , 1991, **1**, 521- .

[17] R. Ross, and P. Pincus, *Macromolecules,* 1992, **25** , 2177–2183.

[18] J. Wittmer and J.-F. Joanny, *Macromolecules,* 1993, **26**, 2691-2697 .

[19] O.V. Borisov, E.B. Zhulina and T.M. Birshtein, *Macromolecules,* 1994, **27**, 4795- .

[20] S.J. Miklavic and S. Marcelja, *J. Phys. Chem.,* 1988, **92**, 6718-6722.

[21] S. Misra, S. Varanasi and P.P. Varanasi, *Macromolecules,* 1989, **22**, 4173-4179.

[22] R. Israels, F.A.M. Leermakers, G.J. Fleer and E.B. Zhulina, *Macromolecules,* 1994, **27**, 3249- .

[23] Israels, R,; Leermakers, F.A.M.; Fleer, G.J. *Macromolecules* **1994**, *27,* 3087-3093.

[24] E.B. Zhulina and O.V. Borisov, *J. Chem. Phys.,* 1997, **107**, 5952- .

[25] E.B. Zhulina, J. Klein Wolterink and O.V. Borisov, *Macromolecules,* 2000, **33**, 4945- .

[26] M.W. Matsen, *Eur. Phys. J. E,* 2011, **34** , 45.

[27] S.T. Milner, T.A. Witten, and M.E. Cates, *Macromolecules,* 1989, **22**, 853-861.

[28] N. Dan and M. Tirrell, *Macromolecules* 1993, **26**, 6467-6473.

[29] A.M. Skvortsov, L.I. Klushin and A.A. Gorbunov, *Macromolecules*, 1997, **30**, 1818-1827.

[30] L.I. Klushin, T. M. Birshtein, and V. M. Amoskov, *Macromolecules*, 2001, **34**, 9156-9167.

[31] T.M. Birshtein, Yu.V. Liatskaya and E.B. Zhulina, *Polymer*, 1990, **31**, 2185 - 2196.

[32] S. Qi , L. I. Klushin, A. M. Skvortsov and F. Schmid, *Macromolecules*, 2016, **49**, 9665–9683.

[33] P.Y. Lai and E.B. Zhulina, *Macromolecules* 1992, **25**, 5201- 5207.

[34] Y.-H. Xue, H. Liu, Z.-Y. Lu and X.-Z. Liang, *J. Chem. Phys.,* 2010, **132**, 044903.

[35] D. Romis and J.-U. Sommer, *Appl. Matter. Interfaces,* 2015, **7**, 12496-12504.

[36] R. Levicky, N. Koneripalli, M. Tirrell and S.K. Satija, *Macromolecules*, 1998, **31**, 2616-2621.

[37] E. Kumacheva, J. Klein, P. Pincus and L.J. Fetters, *Macromolecules*, 1993, **26**, 6477-6482.

[38] A.N. Semenov, *Sov. Phys. JETP*, 1985, **61**, 733-742.

[39] G.J. Fleer, M.A. Cohen Stuart, J.M.H.M. Scheutjens, T. Cosgrove and B. Vincent, *Polymers at Interfaces*, Chapman & Hall, London, 1993

[40] P.Y. Lai and E.B. Zhulina, *J Physique II*, 1992, **2**, 547 - 560.

[41] J. Deek, P.J. Chung, J. Kayser, A.R. Bausch and C.R. Safinya, *Nat. Commun.,* 2013, **4**, 2224

[42] J.-F. Leterrier and J. Eyer, *Biochem. J.* 1987, **245**, 93-101.

[43] E.B. Zhulina and F.A.M. Leermakers *Soft Matter* 2009, 5, 2836-2840.

[44] T. Nakagawa, J. Chen, Z. Zhang, Y. Kanai and N. Hirokawa, *J Cell Biol.,* 1995, 129, 411–429.

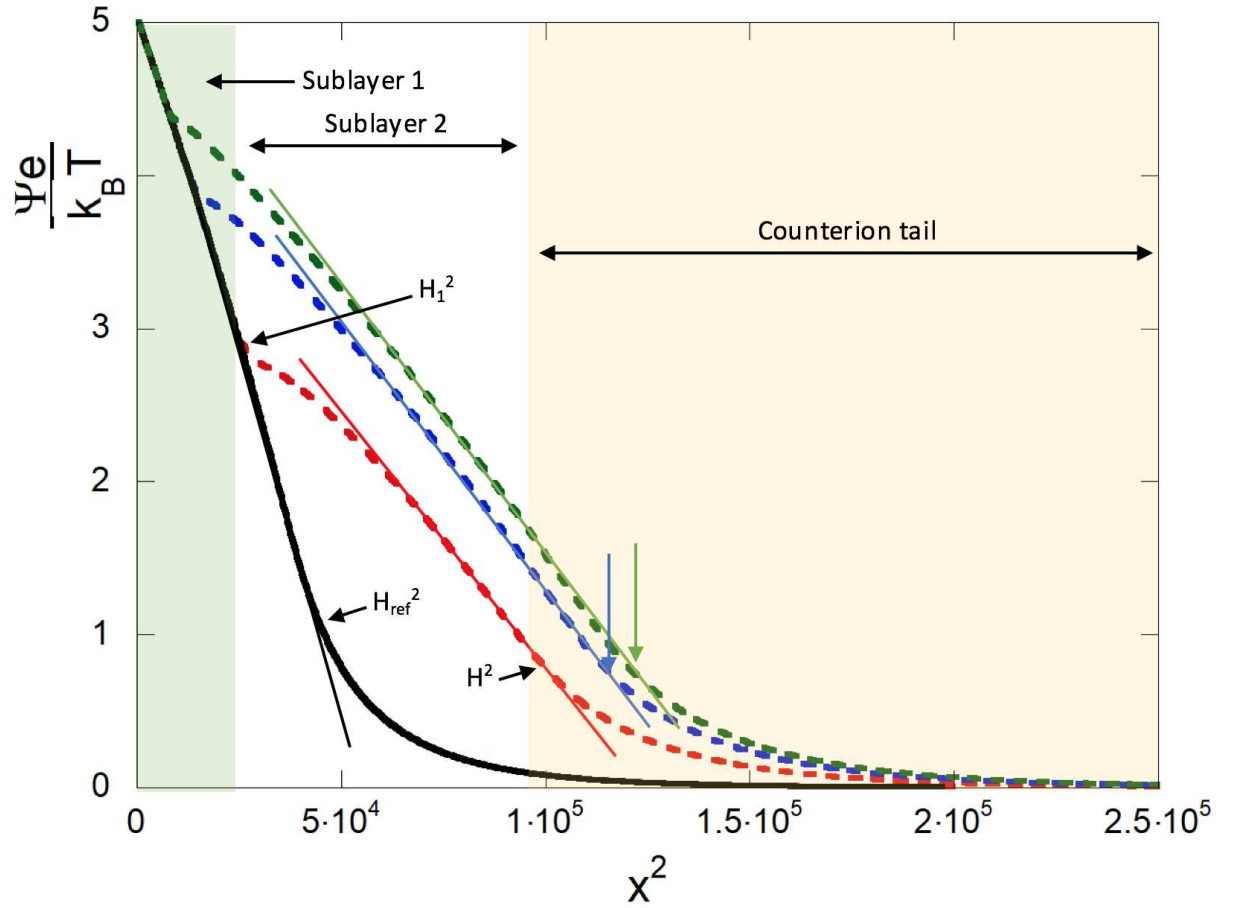[45] N. Srinivasan, M. Bhagawati, B. Ananthanarayanan and S. Kumar, *Nat. Commun.,* 2014, 5, 5145.

Figure 3: Electrostatic potentiual in a reference one-compotent brush with $N_1 = N_2 = 150$ and binary brush with $N_1 = 150$, $N_2 = 500$ and fraction of long chains $q = 01; 03; 05$ plotted as a function of square distance from the surface. The position of the upper edge of the brush H and thickness of the proximal layer H_1 are indicated by arrows.$\sigma = 10^{-3}$. Color code for different values of q explained at the figures.
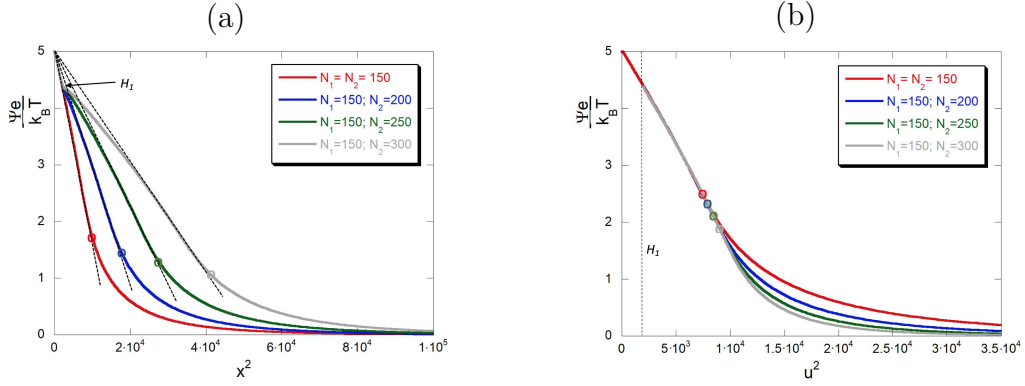
Figure 4: Electrostatic potential in one-component reference polyelectrolyte brush with $N_1 = N_2 = 150$ and binary polyelectrolyte brushes with short chains length $N_1 = 150$ and varied long chains length $N_2 = 200, 250, 300$ at constant fraction $q = 0.5$ of long chains as a function of x^2 (a) and as a function of x^2 in the range $x \leq H_1$ and a function of u^2 in the range $x \geq H_1$ (b).$\sigma = 10^{-3}$. Color code for different N_2 explained at the figures.
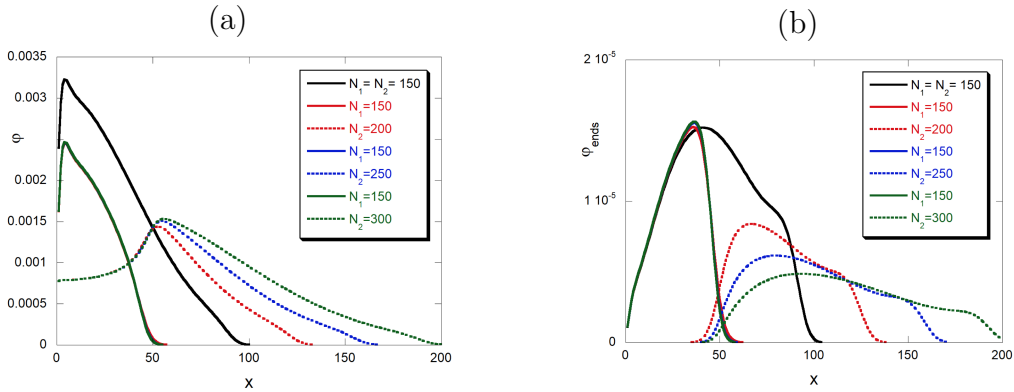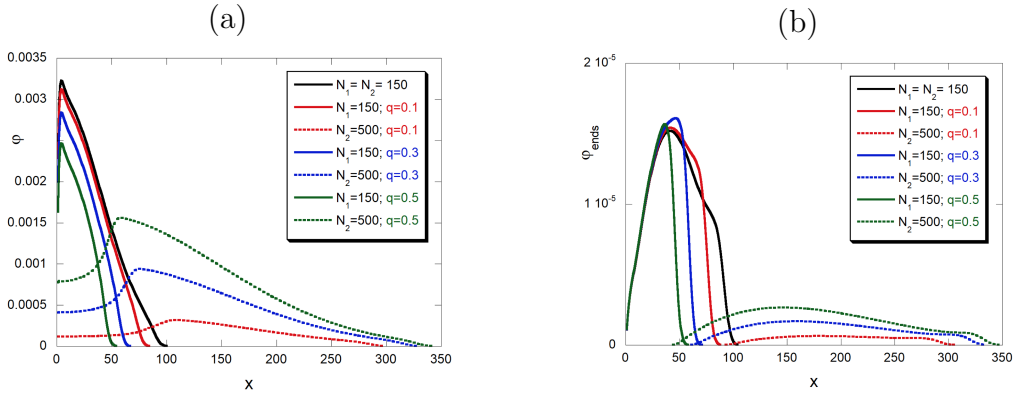

Figure 5: Partial polymer density profiles (a) and distributions of free chain ends (b) in reference one-component polyelectrolyte brush with $N_1 = N_2 = 150$ and binary polyelectrolyte brushes with $N_1 = 150$ and $N_2 = 200, 250, 300$ at constant fraction $q = 0.5$ of long chains, $\sigma = 10^{-3}$. Color code for different N_2 explained at the figures.
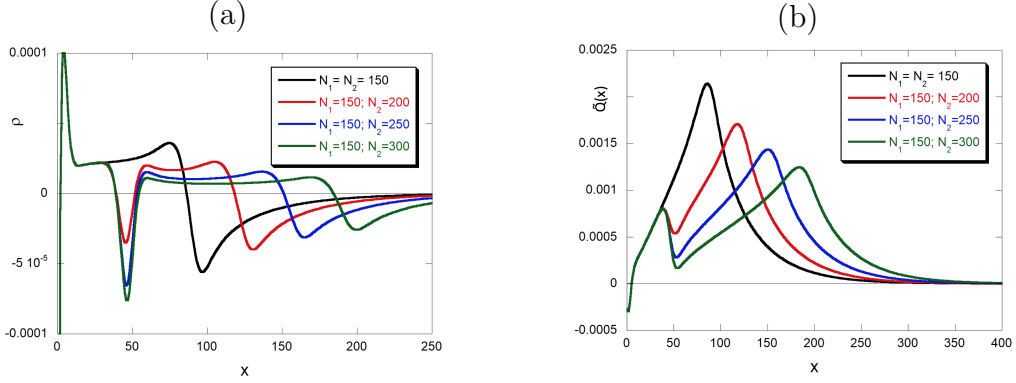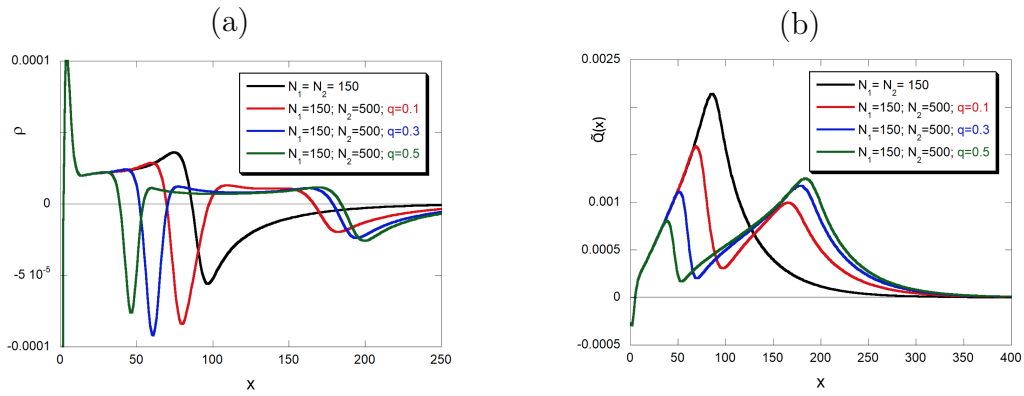
Figure 6: Local net charge density $\rho(x)$ (a) and integral charge $\tilde{Q}(x) = \int_0^x \rho(x')dx'$ per unit area (b) in one-component reference polyelectrolyte brush with $N_1 = N_2 = 150$ and binary polyelectrolyte brushes with short chains length $N_1 = 150$ and varied long chains length $N_2 = 200, 250, 300$ at constant fraction $q = 0.5$ of long chains. $\sigma = 10^{-3}$. Color code for different N_2 explained at the figures.

Figure 7: Partial polymer density profiles (a) and distributions of free chain ends (b) in reference one-component polyelectrolyte brush with $N_1 = N_2 = 150$ and binary polyelectrolyte brushes with $N_1 = 150, N_2 = 500$ at varied fraction $q = 0.1; 0.3; 0.5$ of long chains, $\sigma = 10^{-3}$. Color code for different values of q explained at the figures.
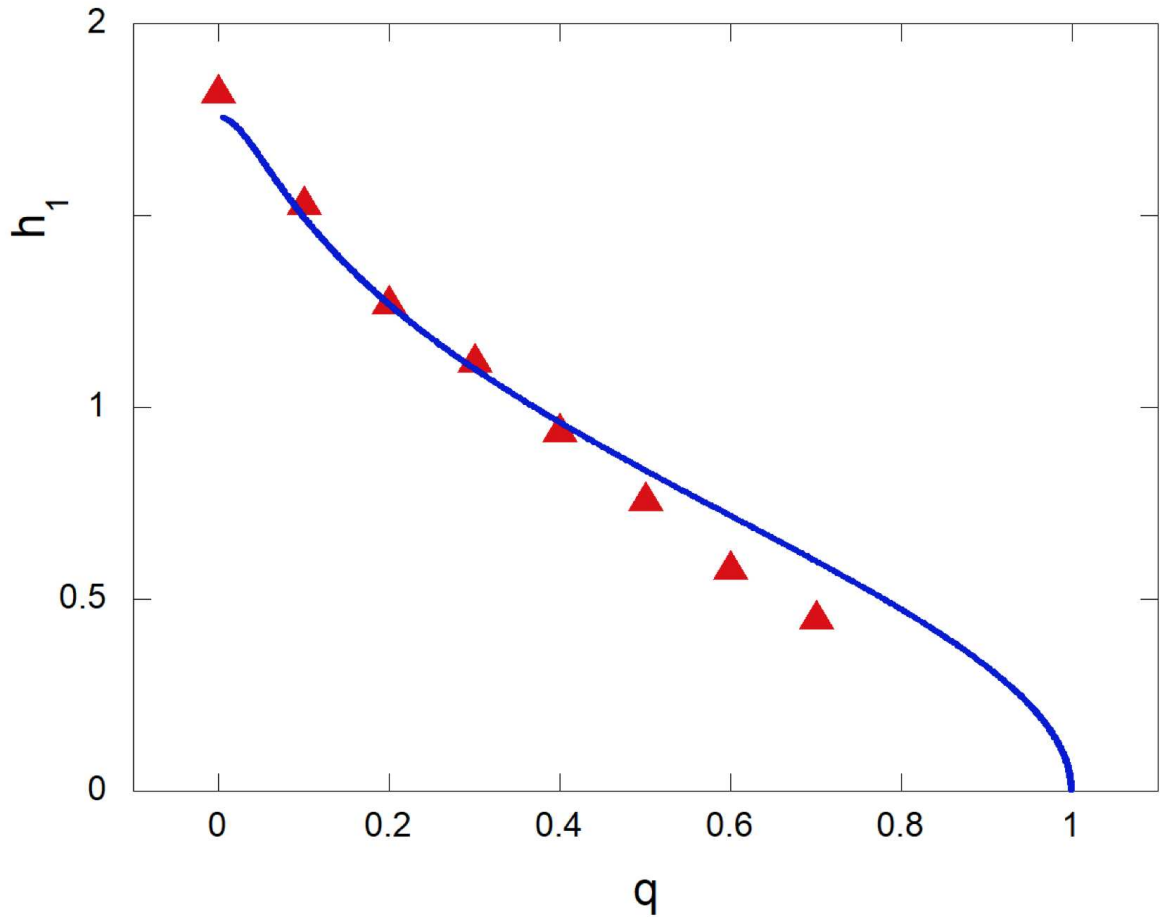
Figure 8: Local net charge density $\rho(x)$ (a) and integral charge $\tilde{Q}(x) = \int_0^x \rho(x')dx'$ per unit area (b) in one-component reference polyelectrolyte brush with $N_1 = N_2 = 150$ and in binary polyelectrolyte brushes with $N_1 = 150, N_2 = 500$ at varied fraction $q = 0.1; 0.3; 0.5$ of long chains. $\sigma = 10^{-3}$. Color code for different values of q explained at the figures.

Figure 9: The reduced thinkness h_1 of the proximal layer in a binary polyelectrolyte brush with $N_1 = 150$, $N_2 = 300$, $\sigma = 10^{-3}$ as a function of fraction q of long chains in the brush. The continuous curve corresponds to the prediction of the analytical theory, eq 24. The points corresponds to the results of the SF-SCF numerical calculations.
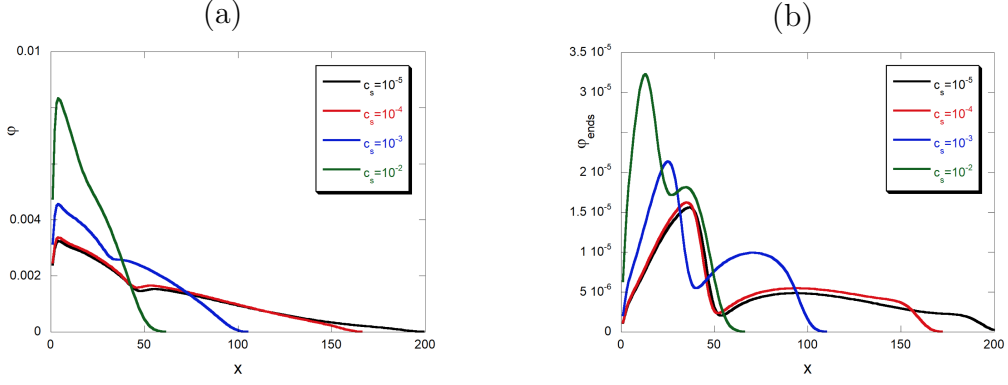
Figure 10: Polymer density profile (a) and free chain ends distribution (b) in binary polyelectrolyte brushes with $N_1 = 150, N_2 = 500$ with the fraction $q = 0.5$ of long chains at varied salt concentration. $\sigma = 10^{-3}$. Color code for different values of salt concentration explained at the figures.
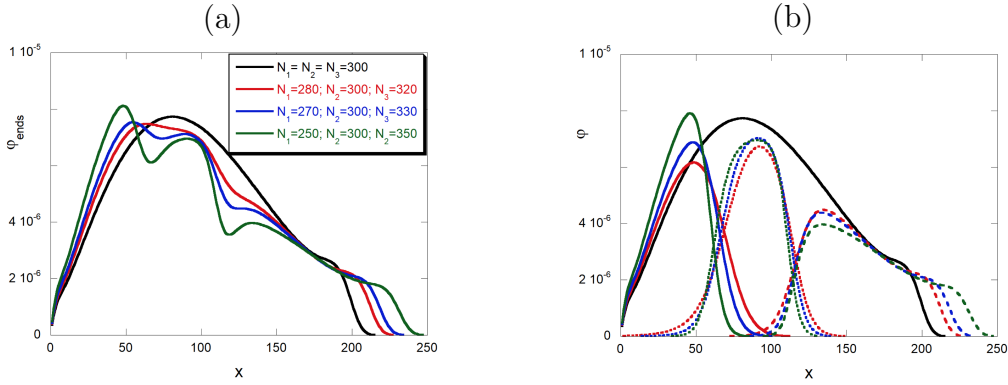

Figure 11: Partial polymer density profiles (a) and distributions of free chain ends (b) in reference one-component polyelectrolyte brush with $N_1 = N_2 = N_3 = 300$ and ternary polyelectrolyte brushes with $N_2 = 300$ and varied length of shorter, $N_1 = 280, 270, 250$, and longer, $N_3 = 900 - N_1 - N_2 = 320, 330, 350$ chains. The fractions $q_1 = q_2 = q_3 = 1/3$ of chains of different lengths are the same. $\sigma = 10^{-3}$. Color code for different values of N_1 and N_3 explained at the figures.
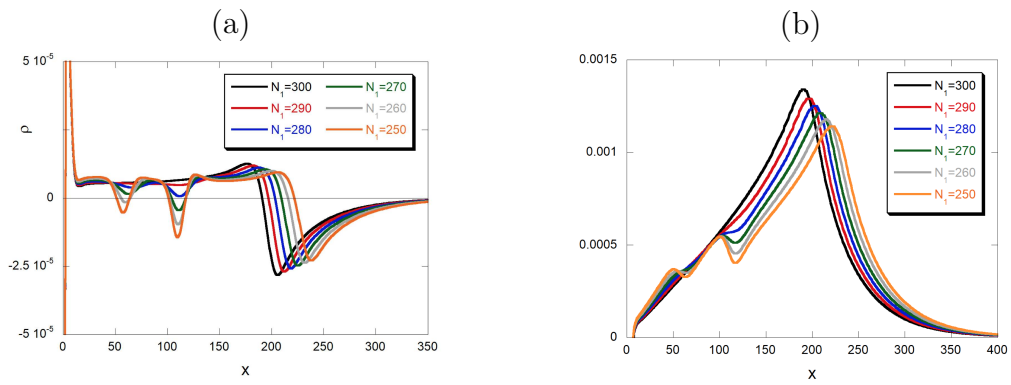
Figure 12: Local net charge density $\rho(x)$ (a) and integral charge $\tilde{Q}(x) = \int_0^x \rho(x')dx'$ per unit area (b) in one-component reference polyelectrolyte brush with $N_1 = N_2 = N_3 = 300$ and in ternary polyelectrolyte brushes at varied lengths N_1 and N_3 of shorter and longer chains, respectively. Other parameters are explained in the legend to Figure 11.